ACS APPLIED MATERIALS & INTERFACES

www.acsami.org

Research Article

InAsP Quantum Dot-Embedded InP Nanowires toward Silicon Photonic Applications

Ting-Yuan Chang, Hyunseok Kim,* William A. Hubbard, Khalifa M. Azizur-Rahman, Jung Jin Ju, Je-Hyung Kim, Wook-Jae Lee,* and Diana Huffaker

Cite This: *ACS Appl. Mater. Interfaces* 2022, 14, 12488–12494

Read Online

ACCESS | Metrics & More | Article Recommendations | Supporting Information

ABSTRACT: Quantum dot (QD) emitters on silicon platforms have been considered as a fascinating approach to building next-generation quantum light sources toward unbreakable secure communications. However, it has been challenging to integrate position-controlled QDs operating at the telecom band, which is a crucial requirement for practical applications. Here, we report monolithically integrated InAsP QDs embedded in InP nanowires on silicon. The positions of QD nanowires are predetermined by the lithography of gold catalysts, and the 3D geometry of nanowire heterostructures is precisely controlled. The InAsP QD forms atomically sharp interfaces with surrounding InP nanowires, which is in situ passivated by InP shells. The linewidths of the excitonic (X) and biexcitonic (XX) emissions from the QD and their power-dependent peak intensities reveal that the proposed QD-in-nanowire structure could be utilized as a non-classical light source that operates at silicon-transparent wavelengths, showing a great potential for diverse quantum optical and silicon photonic applications.

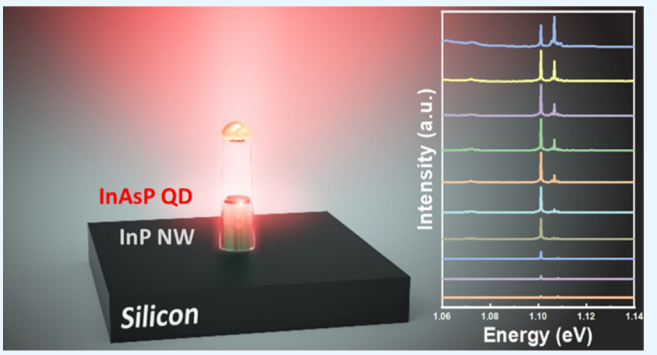

KEYWORDS: *quantum dot-embedded nanowire, InAsP quantum dot, VLS epitaxy, silicon photonics, exciton−biexciton transition*

INTRODUCTION

With the emergence of quantum information science, single and entangled photon sources, which can serve as key components to achieve secure communications via quantum cryptography or quantum key distribution (QKD), have been intensely studied over the last few decades.[1−4] Attenuated laser pulses which is a weak coherent light are widely used as an approximation to a single photon source in QKDs because such classical light sources are easy to prepare by using optical filters. However, attenuated laser pulses occasionally produce multiple photons per pulse which is vulnerable to the photon-number splitting attack without complex architectures such as the decoy state method and therefore the use of pure on-demand single photons is required to ensure high security.[5,6] In addition, miniaturizing quantum devices including quantum light sources has been recognized as a major obstacle because integrated quantum devices on chips can reduce the cost and provide a pathway for various quantum communication protocols.[7]

Epitaxial semiconductor quantum dots (QDs) are particularly attractive in building these on-demand non-classical light sources at telecommunication wavelengths by virtue of the possibility in engineering the band alignment and providing three-dimensional (3D) quantum confinement.[8] A well-known and common approach is self-assembled QDs grown in Stranski−Krastanow (SK) mode on semiconductor thin films that are capped in 3D material matrix.[9,10] This method, however, is challenging to implement due to the randomness in spatial distribution of the position of QDs and the inhomogeneity of QD dimensions. This leads to spectral diffusion and insufficient photon extraction, whereas the development of practical and operable devices requires either a perfect alignment with certain optical components, such as nanophotonic cavity or waveguide, or a small vertical divergence angle for optical fiber coupling.[11,12] To address these issues, a novel method of embedding QDs within bottom-up integrated nanowires is proposed, which can achieve not only self-alignment, but precise positioning by lithographically defined growth site.[13,14] The controllability of the position of QDs by the quantum-dot-in-nanowire (QD-NW) approach is therefore promising for quantum light sources compatible with quantum photonic integrated circuit (QPIC). In addition, bottom-up nanowires have unique advantages in accurate formation of axial and core/shell heterostructures within the nanowires by controlling the

Received: October 31, 2021
Accepted: February 8, 2022
Published: February 17, 2022

https://doi.org/10.1021/acsami.1c21013
ACS Appl. Mater. Interfaces 2022, 14, 12488−12494

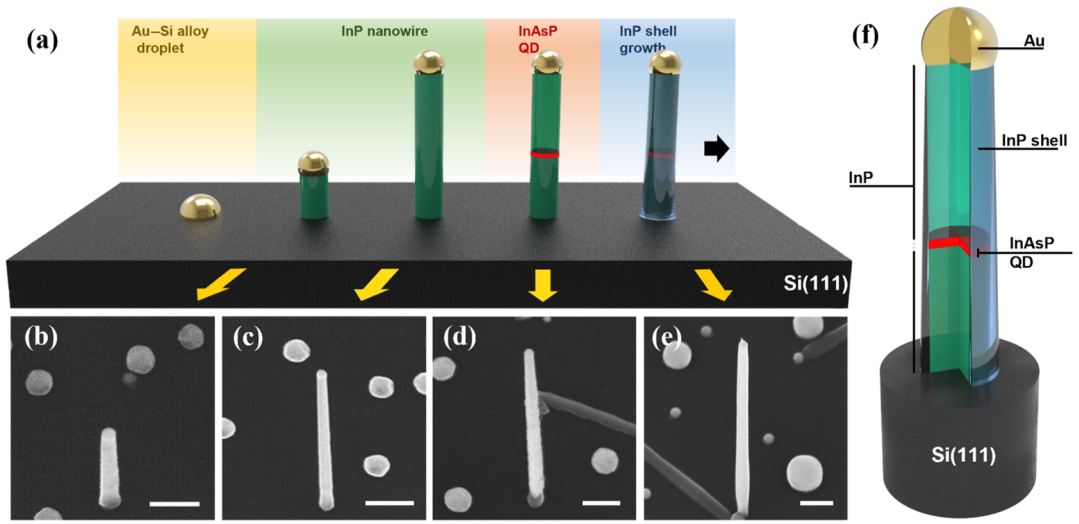

Figure 1. Epitaxy of InP nanowires with InAsP QDs. (a) Schematic illustration of InP nanowires and nanowire heterostructures on silicon, and the corresponding SEMs, (b) short InP segment, (c) elongated InP nanowire, (d) InP nanowire with InAsP QD forming a vertical heterostructure, (e) InAsP QD encapsulated by an InP shell, and (f) its detailed schematic. Scale bars, 200 nm.

diffusion lengths of adatoms and thermodynamics in their growth conditions. It is therefore an enabling technology to form 3D quantized structures, such as vertically/radially stacked QDs and quantum wells,[15−18] with effective in situ passivation that can reduce the nonradiative recombination caused by surface states.[19−21] Another key benefit provided by the QDs grown in vertical nanowires is that the QDs form hexagonally or circularly shaped disks. Such hexagonal or circular geometry provides high degree of structural symmetry (C_{3v}) and can eliminate the fine-structure splitting (FSS), which is crucial in generating polarization-entangled photon pairs.[22] In stark contrast, conventional QDs formed by the SK growth mode exhibit pyramidal shape and experience larger FSS due to the symmetry lower than D_{2d}, which is detrimental for entanglement.[23]

The vapor−liquid−solid (VLS) method is one of the most common and mature techniques in growing bottom-up III−V nanowires incorporating QDs, wherein sharp material interfaces can be realized by precisely controlling the supersaturation of adatoms in catalysts, which is crucial for quantum confinement for exciton−biexciton generation.[13] Within the last couple of decades, significant efforts have been made to grow III−V QD-NWs on a homogeneous substrate and the research focus has been gradually moved onto growing nanowires on silicon platform for silicon photonic applications. Despite the fact that a great leap of progress has been made, most studies to date are demonstrated in GaAs matrix with high surface recombination velocity (~10^6 cm/s), which seriously impairs the quantum efficiency and therefore necessitates the incorporation of capping layers with small lattice mismatch to prevent dephasing.[24−27] AlGaAs is commonly used as in situ capping layer of GaAs matrix, which greatly reduces the surface recombination velocity. However, this is an imperfect solution as Al oxidizes and degrades over time. Although an additional lattice-matched capping layer, such as GaAs, over the AlGaAs shell to form a core/shell/shell structure has been widely adopted, having perfect control on both axial and radial growth rate of the shell layers is a demanding requirement for efficient electrical contact.[28] Besides, another potential limitation of the GaAs/AlGaAs QDs and GaAs/InGaAs QDs is that the emission wavelengths from QDs are typically in the range of 700−1000 nm, which is below the silicon transparency (λ > 1.1 μm), making them less favorable for on-chip integration and long-distance transmission due to attenuation and dispersion loss. In other words, for practical and functional QD-NW quantum emitters, it is necessary to form position-controlled nanowires on a silicon platform operating particularly in the silicon-transparent regime, ideally at telecommunication bands. In this regard, InP nanowires could be a promising building block because InP matrix exhibits much lower surface recombination velocity (~10^3 cm/s) even without passivation and successful ex situ passivation with AlO_x is possible.[25,29−32] Also, by embedding In(As)P QDs in InP nanowires, the emission wavelength can be tuned over a wide range potentially covering the telecom O-band and C-band via tailoring the As composition and QD dimensions, providing an opportunity for prospective electrical contact to InP nanowires and a pathway for deterministic photon pair creation at telecom bands.

In this study, we report on InAsP QDs embedded in InP nanowires grown on a silicon platform by the VLS method that can satisfy those requirements using metal−organic chemical vapor deposition (MOCVD). The optical properties of QDs are probed by cryogenic micro-photoluminescence (μ-PL) setup, from which excitonic (X) and biexcitonic (XX) emissions are observed and the dynamics of exciton−biexciton transitions are identified. The results suggest that the proposed method of forming QD-NWs on silicon can be universally applied to obtain ternary QDs in nanowires covering exciton−biexciton emission wavelength in the telecom regime. In this manner, by forming these nanowires on silicon-on-insulator photonic platforms and waveguides which have been recently reported, the QD-NW emitters can be utilized in silicon photonic applications such as wavelength multiplexed nanowire single photon sources.[33−35]

RESULTS AND DISCUSSION

Nanowire Growth. An undoped 6-inch silicon (111) wafer is adopted as a growth substrate for VLS epitaxy, and gold (Au) nanodot arrays as a growth catalyst are patterned by electron beam (e-beam) lithography and the lift-off process. In

https://doi.org/10.1021/acsami.1c21013
ACS Appl. Mater. Interfaces 2022, 14, 12488−12494

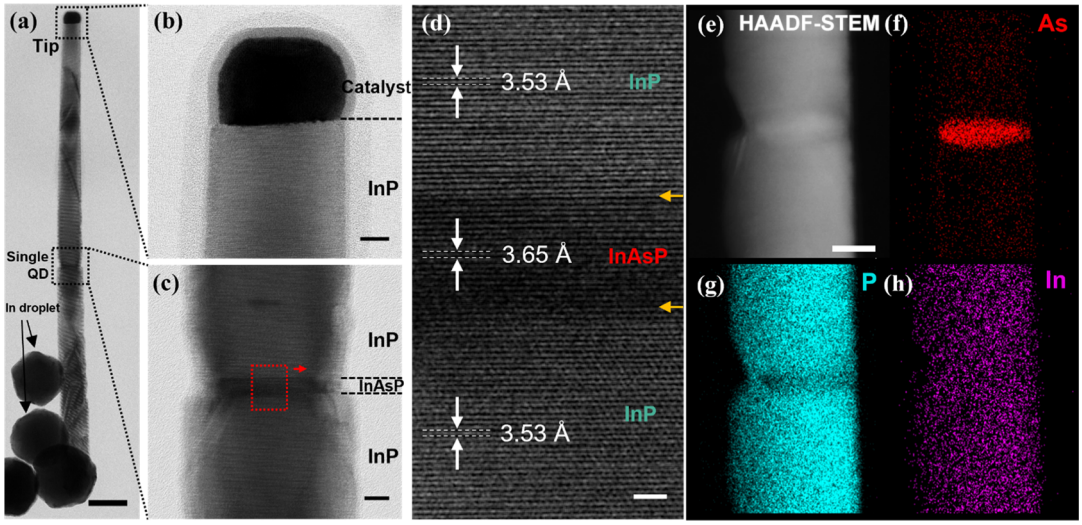

Figure 2. Atomic structure of InAsP QD embedded in InP nanowire. (a) STEM images of nanowire with a single QD, with 100 nm scale bar, and the high-magnification images around the (b) nanowire tip and (c) QD region, with 10 nm scale bars. (d) High-resolution STEM image showing the abrupt InP/InAsP/InP interface with an interplanar spacing of 3.53 Å/3.65 Å/3.53 Å. Scale bar, 2 nm. EDS analysis of InAsP QD in InP nanowire. (e) HAADF-STEM image of nanowire and (f–h) 2-D elemental mapping of As (red), P (cyan), and In (magenta), respectively. Scale bar, 20 nm.

this work, the nanowires are grown by the VLS method using a low-pressure (60 Torr) Emcore D-75 MOCVD reactor, wherein ultra-high purity hydrogen (H_2) is used as a carrier gas for III–V precursors; trimethylindium (TMIn), tertiarybutylphosphine (TBP), and tertiarybutylarsine (TBAs) (see Supporting Information Sections I and II for detailed sample preparation and growth processes). Figure 1 shows the schematic of step-by-step processes to control the geometry of nanowire heterostructures using the VLS method along with the scanning electron microscopy (SEM) images of nanowires corresponding to each step. First, when InP nanowires are grown at 420 °C with a V/III flow rate ratio of 760, the nanowires grown for 5 min and for 10 min show almost identical diameters with different heights (Figure 1b,c), representing growth that is purely vertical under this growth condition. Based on these results, InP–InAsP QD-InP vertical heterostructure is grown by first growing a short stem of InP nanowire, followed by QD formation by a pulsed flow of TBAs, and then vertical overgrowth of InP segment on top (Figure 1d). For QD formation, TMIn and TBP flows are shut down during the pulsed flow of TBAs, which has enabled the formation of QDs with atomically sharp interfaces by the reservoir effect of Au catalysts (see Supporting Information Section II and V for details). Nearly no radial increment is found from the short segment of InP nanowire (radius ~66.3 nm) to the growth of InAsP QD embedded in InP nanowire (radius ~67.7 nm) with the same growth temperature, as shown in Figure 1b–d. Because the nanowire aspect ratio and morphology are determined by competition between the radial and axial growth rate, this shows that the radial growth rate is suppressed by maintaining the growth temperature. According to Paiman et al. and Zhong et al., tapered nanowires are formed at high growth temperatures because the surface diffusion of adatom is kinetically favorable to incorporate in the nanowire by the vapor–solid mechanism under high growth temperature.[36,37] Indeed, when the growth temperature of the upper InP segment is increased to 460 °C after forming InAsP QD, a slightly tapered InP shell can be overgrown on the InP nanowire surrounding the QD (Figure 1e), unlike the fully axial growth mode as shown in Figure 1d. The thin InP shell provides a 3D carrier confinement and passivation for the InAsP QD as schematically depicted in Figure 1f, which is employed as the structure for quantum emitters in this study. It is worth mentioning that, by controlling the growth condition, the InP shell can be grown to form a needle shape, which can be utilized in tailoring the output divergence angle to improve the collection efficiency to external optics.[38,39] Here, even though we have achieved the integration of hybrid QD-NWs on a silicon platform, the growth yield in Figure 1b–e is relatively low. We envision that the growth yield on silicon can be improved by modifying the growth template and by tuning the growth condition (See Supporting Information Section IV for detailed discussion).

Atomic Structures of QD-NWs. The as-grown InP vertical nanowire with InAsP single QD is mechanically broken and transferred to a copper grid for scanning transmission electron microscopy (STEM) and energy-dispersive X-ray spectroscopy (EDS) analyses (see the Supporting Information for EDS analysis of the catalyst/nanowire interface). For gaining clear insights into InP/InAsP/InP interfaces as well as material compositions of InAsP QD, the nanowire without InP shell as depicted in Figure 1d is used in the material studies given that the shell can simultaneously generate the In and P counts during the EDS scan. Figure 2a shows the bright-field STEM image of a purely axial InP/InAsP/InP nanowire heterostructure with the diameter and length of approximately 63 nm and 1.26 μm, respectively. Several parasitic In droplets that are formed during the growth are shown together. The high-magnification STEM images of nanowire tips and single InAsP QD are shown in Figure 2b,c, in which the InP/InAsP/InP sharp material interfaces can be clearly observed. In order to confirm the interface quality, high-resolution STEM is performed to capture the InP/InAsP/InP interfaces, which are labeled with yellow arrows as shown in Figure 2d. The QD with a thickness of 6.94 nm is composed of 19 InAsP monolayers with an equal interspacing of 3.65 Å (*d*-spacing), and it is sandwiched by InP layers with an atomically abrupt interface.

https://doi.org/10.1021/acsami.1c21013
ACS Appl. Mater. Interfaces 2022, 14, 12488–12494

Next, the two-dimensional elemental mapping of the InAsP QD region using the EDS technique is plotted as shown in Figure 2f–h. Figure 2e–h presents the high-angle annular dark-field scanning transmission electron microscopy (HAADF-STEM) image and the corresponding material distribution of As (red), P (cyan), and In (magenta) along the heterointerface, respectively. It can be clearly seen that In is spreading uniformly in the entire nanowire, whereas As is tightly appearing in the QD region replacing the P sites to form $InAs_xP_{1-x}$ with an estimated composition of $x = 0.6$, which corresponds to a bulk energy gap of $E_g \sim 0.724$ eV. It should be noted that the slight spreading of As is not caused by the material diffusion, but by an offset angle in the STEM rotational setup which is set to reduce the false signal collected from the TEM copper grid. With both results of STEM and EDS scanning, it is therefore confirmed that the InP/InAsP interfaces are atomically sharp without crystal defects, forming high-quality QDs. InP/InAsP QDs form type-I band alignment, and the emission wavelength of the InAsP QD can be tailored by both the ternary material composition and the QD size owing to the quantum confinement effect, which shows great promise in building wavelength-tunable non-classical quantum emitters.[40]

Optical Properties of QD-NWs. The optical properties of InAsP QDs in InP nanowires are probed using a cryogenic μ-PL setup at 4K (see Supporting Information Section III for the detailed optical characterization setup). As seen in Figure 2a and in Supporting Information Figure S3, the silicon surface is partially contaminated by randomly formed droplets. As a consequence, it is critical to measure the spectrum of background and use it as a reference to subtract from the QD-NW emission spectra. Nevertheless, we did not observe any spectral features between 0.77 and 1.38 eV (900–1600 nm) within the scope of this study. Thus, we can assume that the optical emission is solely from the QD-NW segments. μ-PL and time-resolved photoluminescence (TRPL) are measured from as-grown vertical nanowires without transferring them onto foreign substrates. In Figure 3a, a silicon-transparent emission at 1.109 eV is observed with a sharp linewidth of 267.4 μeV from the InAsP QDs, which is lower than the thermal broadening of $k_BT \sim 344.7$ μeV, indicating a discrete nature of energy states of the InAsP QDs. In addition, the emission with a larger energy splitting than the bulk energy gap ($E_g \sim 0.724$ eV) confirms the strong spatial confinement of carriers provided by the InAsP quantized structure. Next, the time evolution of the InAsP QDs in InP nanowires is examined by TRPL measurement, where the same setup of μ-PL is used along with a single-photon detector. Because InP is known for low surface recombination velocity and the QD excitonic emissions could partially be coupled to the HE_{11} mode provided by the nanowire waveguide,[41] the carrier lifetime measured by TRPL is a manifestation of both the material properties of the QD-NW and the geometric effect from nanowires.[25] Figure 3b exhibits a slow decay with an extracted lifetime of 20.422 ns. This is in good agreement with the reported high-quality InAsP QDs embedded in InP nanowires, where the spontaneous emission is mainly attributed to the non-guided radiative modes propagating randomly away from the nanowire.[41,42] The long decay time also serves as a compelling evidence of strong 3D confinement of well-passivated InAsP QDs embedded in vertically standing InP nanowires.

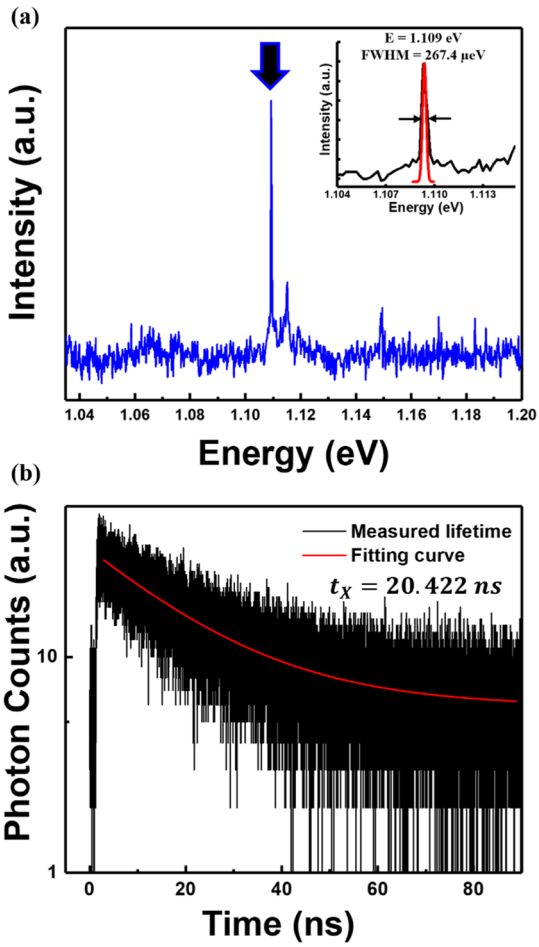

Figure 3. (a) Emission spectra from the QD-NW at 4K. Inset: linewidth fitting of the peak. (b) TRPL measurement of the sharp emission at $E = 1.109$ eV with an extracted lifetime of 20.422 ns.

Figure 4a shows the power dependency of InAsP QD emission at 4K environment with the pump power increasing from 200 nW to 200 μW. Three extremely narrow peaks can be clearly seen starting at the excitation power of 20 μW. Here, we denote the two sharp peaks as—an excitonic line (X) at ~1.101 eV and a biexcitonic line (XX) at ~1.107 eV, in which the X line and XX line exhibit the full width at half-maximum of 219.2 and 244.6 μeV by Lorentzian curve fitting. The measured excitonic and biexcitonic peak linewidths have similar orders compared to other reported nanowire QDs.[27,39,43] However, these values are approximately 1-to-2 orders higher than that of the conventional planar self-assembled QDs.[44] The linewidth broadening of the QDs in nanowires is typically caused by the fluctuation of charges in the vicinity of QDs.[45] Such a phenomenon can be associated with the surface states and crystal defects such as stacking faults, creating a series of carrier trapping and detrapping process, which are often formed in bottom-up nanowires.[46,47] Also, the strain induced by the native oxide shell could play a role in the spectral broadening of QDs.[48] The intensity of the excitonic emission (I_X) and biexcitonic emission (I_{XX}) as a function of the excitation power (P) is plotted as shown in Figure 4b in double logarithmic scales. As the excitation power increases, the excitonic line starts to show intensity saturation when the biexcitonic line appears. I_X has a sublinear dependency with the excitation power ($\propto P^{0.72}$), whereas I_{XX}

https://doi.org/10.1021/acsami.1c21013
ACS Appl. Mater. Interfaces 2022, 14, 12488–12494

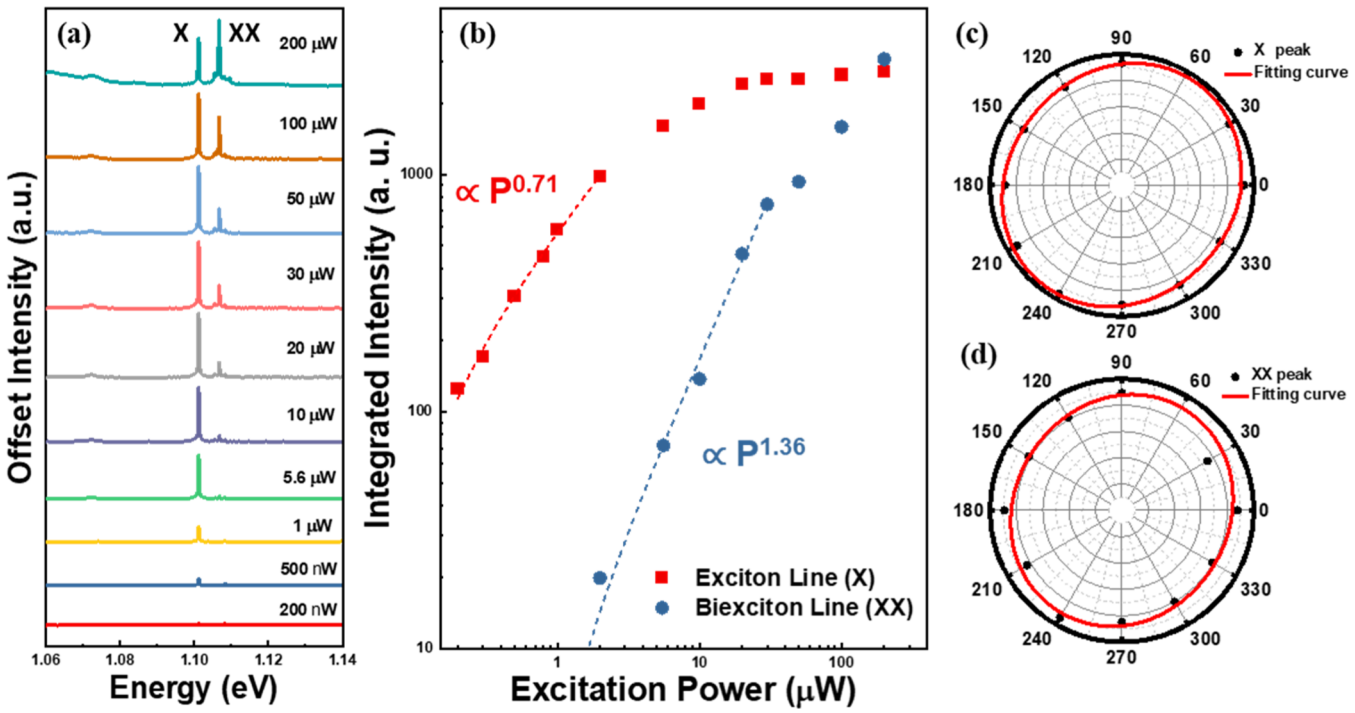

Figure 4. Optical characteristics of InAsP QD in InP nanowire. (a) Power-dependent emission spectra of the QD-NW when the pump power is increased from 0.2 W to 200 μW. The neutral excitonic and biexcitonic lines are indicated as X and XX, respectively. (b) Peak intensities of exciton (X) and biexciton peak (XX) as a function of the excitation power. (c) Polarization-dependent peak intensities of excitonic peak (X) and (d) biexcitonic peak (XX) at the excitation power of 20 μW.

has a superlinear dependency with the excitation power ($\propto P^{1.36}$). The exponent of I_{XX} is ~1.89 times higher than that of I_X, which is a direct clue and signature property of biexciton and exciton transitions.

Lastly, the polarization properties of the QD emission lines are investigated at 4K. The measured polarization distributions and the fitting curves of the excitonic line (X) and the biexcitonic line (XX) are illustrated in Figure 4c. The emission from the vertical nanowire, denoted as $+z$ direction, is collected through a half waveplate without the presence of external fields. In general, the polarization property, determined by the orientation of dipole moments, contains E_x and E_y components in the in-plane direction of nanowire cross section. As reported elsewhere, nanowires with an elongated cross section can drastically increase the non-degeneracy of the two components.[49] In other words, the polarization perpendicular to the nanowire axis generally exhibits very low degree of polarization.[50,51] Thus, X and XX emission lines in Figure 4c from the vertical nanowire show a very weak intensity variation along the angle of linear polarization, which indicates that X and XX emission peaks are from the vertically standing and symmetric nanowire. With this regard, the vertical nanowire in this study not just provides the 3D quantum confinement, but also preserves the genuine and intrinsic optical properties of QDs without perturbing the polarizations, which would be an ideal platform for entangled photon generation as well as single photon generation.

CONCLUSIONS

In conclusion, we have demonstrated the monolithic integration of InAsP QDs in InP nanowires on silicon substrates using the VLS method. The atomic abruptness of the InP/InAsP interface formed by a pulsed growth mode is analyzed via the STEM and EDS technique, which is crucial in forming high-quality QDs. The signature of QDs with narrow optical transitions has been observed, and the cryogenic μ-PL measurement clearly showed the exciton−biexciton transitions in the InAsP QDs. In addition, the exciton and biexciton emission wavelengths are potentially tunable by the QD size or ternary material composition in the silicon-transparent regime. This study provides a promising foundation for further developing site-controlled non-classical light sources for future quantum integrated technologies.

EXPERIMENTAL SECTION

Au Nanodot Patterning for VLS Epitaxy. Si(111) wafers are first cleaned by Piranha solution and 6:1 buffered oxide etchant solution. Next, nanohole patterns are defined on e-beam resist (PMMA 950A2) using Raith EBPG5000 ES e-beam writer, by a standard e-beam lithography process. After exposure and developing in MIBK/IPA = 1:3 solution, Au is deposited by e-beam evaporation with a nominal thickness of 15 nm. Finally, the Au nanodots are formed by the lift-off process using NMP (1-Methyl-2-pyrrolidon) and then washing with IPA.

Nanowire Epitaxy. The growth is carried out in a MOCVD reactor (Emcore D-75) at 60 Torr using hydrogen as the carrier gas. TMIn, TBP, and TBAs are used as precursors for In, P, and As, respectively. After ramping up the temperature to the growth temperature of 420 °C without flowing any precursors, TBP and TMIn are simultaneously turned on to initiate the growth of InP segments. Then, the InAsP QDs are formed by shutting off TMIn and TBP and turning on TBAs, all at the same time, for 1 s. For the growth of upper InP segments, the growth temperature is kept at 420 °C for purely vertical growth or increased to 460 °C for sidewall passivation. After the growth, the reactor is cooled down with TBP flow to prevent the desorption of nanowires. Further details on the patterning, epitaxy, and characterization can be found in the Supporting Information.

https://doi.org/10.1021/acsami.1c21013
ACS Appl. Mater. Interfaces 2022, 14, 12488−12494

■ ASSOCIATED CONTENT

Supporting Information

The Supporting Information is available free of charge at https://pubs.acs.org/doi/10.1021/acsami.1c21013.

Detailed sample preparation processes, nanowire epitaxy, optical measurement setup, growth results and discussion, and EDS analysis (PDF)

■ AUTHOR INFORMATION

Corresponding Authors

Hyunseok Kim − *Department of Electrical and Computer Engineering, University of California Los Angeles, Los Angeles, California 90095, United States; Department of Mechanical Engineering, Massachusetts Institute of Technology, Cambridge, Massachusetts 02139, United States;* orcid.org/0000-0003-3091-8413; Email: hyunseokkim@ucla.edu

Wook-Jae Lee − *Electronics and Telecommunications Research Institute, Daejeon 34129, South Korea; Department of Data Information and Physics, Kongju National University, Gongju 32588, South Korea*; Email: wookjaelee@kongju.ac.kr

Authors

Ting-Yuan Chang − *Department of Electrical and Computer Engineering, University of California Los Angeles, Los Angeles, California 90095, United States*

William A. Hubbard − *NanoElectronic Imaging Inc., Los Angeles, California 90095, United States;* orcid.org/0000-0002-2924-0820

Khalifa M. Azizur-Rahman − *School of Physics and Astronomy, Cardiff University, Cardiff, Wales CF24 3AA, U.K.*

Jung Jin Ju − *Electronics and Telecommunications Research Institute, Daejeon 34129, South Korea*

Je-Hyung Kim − *Department of Physics, Ulsan National Institute of Science and Technology (UNIST), Ulsan 44919, South Korea;* orcid.org/0000-0002-6894-9285

Diana Huffaker − *Department of Electrical and Computer Engineering, University of California Los Angeles, Los Angeles, California 90095, United States; School of Physics and Astronomy, Cardiff University, Cardiff, Wales CF24 3AA, U.K.; Department of Electrical Engineering, University of Texas at Arlington, Arlington, Texas 76019, United States*

Complete contact information is available at: https://pubs.acs.org/10.1021/acsami.1c21013

Author Contributions

H.K., W.-J.L., and D.H. conceived the experimental work. T.-Y.C. and H.K. conducted nanowire epitaxy. T.-Y.C. and W.A.H. conducted STEM and EDS measurements. T.-Y.C., J.J.J, J.-H.K, and W.-J.L performed optical characterizations. T.-Y.C. and K.M.A-R. performed data analysis and fitting. The manuscript was written through contributions of all authors.

Notes

The authors declare no competing financial interest.

■ ACKNOWLEDGMENTS

This work was financially supported by the National Science Foundation (through ECCS-1810548), Institute for Information & Communications Technology Promotion (IITP), and the National Research Foundation of Korea (NRF) grants funded by the Korea government (MSIT) (no. 20170000740011001, A Generic Technology Study for QPICs, NRF-2017R1E1A1A01075263). The authors gratefully thank helpful discussions with Sêr Cymru National Research Network (NRN) in Advanced Engineering and Materials and the Mesoscopic Optics and Quantum Electronics Laboratory at UCLA.

■ REFERENCES

(1) Basset, F. B.; Valeri, M.; Roccia, E.; Muredda, V.; Poderini, D.; Neuwirth, J.; Spagnolo, N.; Rota, M. B.; Carvacho, G.; Sciarrino, F.; Trotta, R. Quantum Key Distribution with Entangled Photons Generated on Demand by a Quantum Dot. *Sci. Adv.* **2021**, *7*, abe6379.

(2) Ekert, A. K. Quantum Cryptography Based on Bell's Theorem. *Phys. Rev. Lett.* **1991**, *67*, 661−663.

(3) Jennewein, T.; Simon, C.; Weihs, G.; Weinfurter, H.; Zeilinger, A. Quantum Cryptography with Entangled Photons. *Phys. Rev. Lett.* **2000**, *84*, 4729−4732.

(4) Waks, E.; Inoue, K.; Santori, C.; Fattal, D.; Vuckovic, J.; Solomon, G. S.; Yamamoto, Y. Secure Communication: Quantum Cryptography with a Photon Turnstile. *Nature* **2002**, *420*, 762.

(5) Lütkenhaus, N. Security against Individual Attacks for Realistic Quantum Key Distribution. *Phys. Rev. A* **2000**, *61*, 052304.

(6) Brassard, G.; Lütkenhaus, N.; Mor, T.; Sanders, B. C. Limitations on Practical Quantum Cryptography. *Phys. Rev. Lett.* **2000**, *85*, 1330−1333.

(7) Zhang, G.; Haw, J. Y.; Cai, H.; Xu, F.; Assad, S. M.; Fitzsimons, J. F.; Zhou, X.; Zhang, Y.; Yu, S.; Wu, J.; Ser, W.; Kwek, L. C.; Liu, A. Q. An Integrated Silicon Photonic Chip Platform for Continuous-Variable Quantum Key Distribution. *Nat. Photonics* **2019**, *13*, 839−842.

(8) Senellart, P.; Solomon, G.; White, A. High-Performance Semiconductor Quantum-Dot Single-Photon Sources. *Nat. Nanotechnol.* **2017**, *12*, 1026−1039.

(9) Goldstein, L.; Glas, F.; Marzin, J. Y.; Charasse, M. N.; Le Roux, G. Growth by Molecular-Beam Epitaxy and Characterization of InAs/GaAs Strained-Layer Superlattices. *Appl. Phys. Lett.* **1985**, *47*, 1099−1101.

(10) Leonard, D.; Krishnamurthy, M.; Reaves, C. M.; Denbaars, S. P.; Petroff, P. M. Direct Formation of Quantum-Sized Dots from Uniform Coherent Islands of InGaAs on GaAs-Surfaces. *Appl. Phys. Lett.* **1993**, *63*, 3203−3205.

(11) Badolato, A.; Hennessy, K.; Atatüre, M.; Dreiser, J.; Hu, E.; Petroff, P. M.; Imamoglu, A. Deterministic Coupling of Single Quantum Dots to Single Nanocavity Modes. *Science* **2005**, *308*, 1158−1161.

(12) Arcari, M.; Söllner, I.; Javadi, A.; Lindskov Hansen, S.; Mahmoodian, S.; Liu, J.; Thyrrestrup, H.; Lee, E. H.; Song, J. D.; Stobbe, S.; Lodahl, P. Near-Unity Coupling Efficiency of a Quantum Emitter to a Photonic Crystal Waveguide. *Phys. Rev. Lett.* **2014**, *113*, 093603.

(13) Dick, K. A.; Bolinsson, J.; Borg, B. M.; Johansson, J. Controlling the Abruptness of Axial Heterojunctions in III-V Nanowires: Beyond the Reservoir Effect. *Nano Lett.* **2012**, *12*, 3200−3206.

(14) Lauhon, L. J.; Gudiksen, M. S.; Wang, D.; Lieber, C. M. Epitaxial Core-Shell and Core-Multishell Nanowire Heterostructures. *Nature* **2002**, *420*, 57−61.

(15) Heiss, M.; Fontana, Y.; Gustafsson, A.; Wüst, G.; Magen, C.; O'Regan, D. D.; Luo, J. W.; Ketterer, B.; Conesa-Boj, S.; Kuhlmann, A. V.; Houel, J.; Russo-Averchi, E.; Morante, J. R.; Cantoni, M.; Marzari, N.; Arbiol, J.; Zunger, A.; Warburton, R. J.; Fontcuberta i Morral, A. Self-Assembled Quantum Dots in a Nanowire System for Quantum Photonics. *Nat. Mater.* **2013**, *12*, 439−444.

(16) Lu, F.; Bhattacharya, I.; Sun, H.; Tran, T.-T. D.; Ng, K. W.; Malheiros-Silveira, G. N.; Chang-Hasnain, C. Nanopillar Quantum Well Lasers Directly Grown on Silicon and Emitting at Silicon-Transparent Wavelengths. *Optica* **2017**, *4*, 717−723.

(17) Saxena, D.; Jiang, N.; Yuan, X.; Mokkapati, S.; Guo, Y.; Tan, H. H.; Jagadish, C. Design and Room-Temperature Operation of GaAs/AlGaAs Multiple Quantum Well Nanowire Lasers. *Nano Lett.* **2016**, *16*, 5080−5086.
(18) Tatebayashi, J.; Kako, S.; Ho, J.; Ota, Y.; Iwamoto, S.; Arakawa, Y. Room-Temperature Lasing in a Single Nanowire with Quantum Dots. *Nat. Photonics* **2015**, *9*, 501−505.
(19) Ren, D.; Azizur-Rahman, K. M.; Rong, Z.; Juang, B.-C.; Somasundaram, S.; Shahili, M.; Farrell, A. C.; Williams, B. S.; Huffaker, D. L. Room-Temperature Midwavelength Infrared InAsSb Nanowire Photodetector Arrays with Al_2O_3 Passivation. *Nano Lett.* **2019**, *19*, 2793−2802.
(20) Svensson, C. P. T.; Mårtensson, T.; Trägårdh, J.; Larsson, C.; Rask, M.; Hessman, D.; Samuelson, L.; Ohlsson, J. Monolithic GaAs/InGaP Nanowire Light Emitting Diodes on Silicon. *Nanotechnology* **2008**, *19*, 305201.
(21) Treu, J.; Stettner, T.; Watzinger, M.; Morkötter, S.; Döblinger, M.; Matich, S.; Saller, K.; Bichler, M.; Abstreiter, G.; Finley, J. J.; Stangl, J.; Koblmüller, G. Lattice-Matched InGaAs-InAlAs Core-Shell Nanowires with Improved Luminescence and Photoresponse Properties. *Nano Lett.* **2015**, *15*, 3533−3540.
(22) Singh, R.; Bester, G. Nanowire Quantum Dots as an Ideal Source of Entangled Photon Pairs. *Phys. Rev. Lett.* **2009**, *103*, 063601.
(23) Seguin, R.; Schliwa, A.; Rodt, S.; Pötschke, K.; Pohl, U. W.; Bimberg, D. Size-Dependent Fine-Structure Splitting in Self-Organized InAs/GaAs Quantum Dots. *Phys. Rev. Lett.* **2005**, *95*, 257402.
(24) Heinrich, J.; Huggenberger, A.; Heindel, T.; Reitzenstein, S.; Höfling, S.; Worschech, L.; Forchel, A. Single Photon Emission from Positioned GaAs/AlGaAs Photonic Nanowires. *Appl. Phys. Lett.* **2010**, *96*, 211117.
(25) Joyce, H. J.; Docherty, C. J.; Gao, Q.; Tan, H. H.; Jagadish, C.; Lloyd-Hughes, J.; Herz, L. M.; Johnston, M. B. Electronic Properties of GaAs, InAs and InP Nanowires Studied by Terahertz Spectroscopy. *Nanotechnology* **2013**, *24*, 214006.
(26) Zhang, Y.; Velichko, A. V.; Fonseka, H. A.; Parkinson, P.; Gott, J. A.; Davis, G.; Aagesen, M.; Sanchez, A. M.; Mowbray, D.; Liu, H. Defect-Free Axially Stacked GaAs/GaAsP Nanowire Quantum Dots with Strong Carrier Confinement. *Nano Lett.* **2021**, *21*, 5722−5729.
(27) Wu, J.; Ramsay, A.; Sanchez, A.; Zhang, Y.; Kim, D.; Brossard, F.; Hu, X.; Benamara, M.; Ware, M. E.; Mazur, Y. I.; Salamo, G. J.; Aagesen, M.; Wang, Z.; Liu, H. Defect-Free Self-Catalyzed GaAs/GaAsP Nanowire Quantum Dots Grown on Silicon Substrate. *Nano Lett.* **2016**, *16*, 504−511.
(28) Komolibus, K.; Scofield, A. C.; Gradkowski, K.; Ochalski, T. J.; Kim, H.; Huffaker, D. L.; Huyet, G. Improved Room-Temperature Luminescence of Core-Shell InGaAs/GaAs Nanopillars Via Lattice-Matched Passivation. *Appl. Phys. Lett.* **2016**, *108*, 061104.
(29) Black, L. E.; Cavalli, A.; Verheijen, M. A.; Haverkort, J. E. M.; Bakkers, E. P. A. M.; Kessels, W. M. M. Effective Surface Passivation of InP Nanowires by Atomic-Layer-Deposited Al_2O_3 with PO_x Interlayer. *Nano Lett.* **2017**, *17*, 6287−6294.
(30) Casey, H. C.; Buehler, E. Evidence for Low Surface Recombination Velocity on N-Type InP. *Appl. Phys. Lett.* **1977**, *30*, 247−249.
(31) Nolte, D. D. Surface Recombination, Free-Carrier Saturation, and Dangling Bonds in InP and GaAs. *Solid State Electron.* **1990**, *33*, 295−298.
(32) Rosenwaks, Y.; Shapira, Y.; Huppert, D. Evidence for Low Intrinsic Surface-Recombination Velocity on P-Type InPEvidence for low intrinsic surface-recombination velocity onp-type InP. *Phys. Rev. B: Condens. Matter Mater. Phys.* **1991**, *44*, 13097−13100.
(33) Kim, H.; Lee, W.-J.; Farrell, A. C.; Morales, J. S. D.; Senanayake, P.; Prikhodko, S. V.; Ochalski, T. J.; Huffaker, D. L. Monolithic InGaAs Nanowire Array Lasers on Silicon-on-Insulator Operating at Room Temperature. *Nano Lett.* **2017**, *17*, 3465−3470.
(34) Kim, H.; Lee, W. J.; Chang, T. Y.; Huffaker, D. L. Room-Temperature InGaAs Nanowire Array Band-Edge Lasers on Patterned Silicon-on-Insulator Platforms. *Phys. Status Solidi RRL* **2019**, *13*, 1800489.
(35) Chang, T. Y.; Kim, H.; Zutter, B. T.; Lee, W. J.; Regan, B. C.; Huffaker, D. L. Orientation-Controlled Selective-Area Epitaxy of III-V Nanowires on (001) Silicon for Silicon Photonics. *Adv. Funct. Mater.* **2020**, *30*, 2002220.
(36) Paiman, S.; Gao, Q.; Joyce, H. J.; Kim, Y.; Tan, H. H.; Jagadish, C.; Zhang, X.; Guo, Y.; Zou, J. Growth Temperature and V/III Ratio Effects on the Morphology and Crystal Structure of InP Nanowires. *J. Phys. D: Appl. Phys.* **2010**, *43*, 445402.
(37) Zhong, Z.; Li, X.; Wu, J.; Li, C.; Xie, R. B.; Yuan, X.; Niu, X.; Wang, W.; Luo, X.; Zhang, G.; Wang, Z. M.; Tan, H. H.; Jagadish, C. Wavelength-Tunable InAsP Quantum Dots in InP Nanowires. *Appl. Phys. Lett.* **2019**, *115*, 053101.
(38) Bulgarini, G.; Reimer, M. E.; Bouwes Bavinck, M.; Jöns, K. D.; Dalacu, D.; Poole, P. J.; Bakkers, E. P. A. M.; Zwiller, V. Nanowire Waveguides Launching Single Photons in a Gaussian Mode for Ideal Fiber Coupling. *Nano Lett.* **2014**, *14*, 4102−4106.
(39) Jaffal, A.; Redjem, W.; Regreny, P.; Nguyen, H. S.; Cueff, S.; Letartre, X.; Patriarche, G.; Rousseau, E.; Cassabois, G.; Gendry, M.; Chauvin, N. InAs Quantum Dot in a Needlelike Tapered InP Nanowire: A Telecom Band Single Photon Source Monolithically Grown on Silicon,. *Nanoscale* **2019**, *11*, 21847−21855.
(40) Zhang, G.; Takiguchi, M.; Tateno, K.; Tawara, T.; Notomi, M.; Gotoh, H. Telecom-Band Lasing in Single InP/InAs Heterostructure Nanowires at Room Temperature. *Sci. Adv.* **2019**, *5*, No. eaat8896.
(41) Bleuse, J.; Claudon, J.; Creasey, M.; Malik, N. S.; Gérard, J.-M.; Maksymov, I.; Hugonin, J.-P.; Lalanne, P. Inhibition, Enhancement, and Control of Spontaneous Emission in Photonic Nanowires. *Phys. Rev. Lett.* **2011**, *106*, 103601.
(42) Bulgarini, G.; Reimer, M. E.; Zehender, T.; Hocevar, M.; Bakkers, E. P. A. M.; Kouwenhoven, L. P.; Zwiller, V. Spontaneous Emission Control of Single Quantum Dots in Bottom-up Nanowire Waveguides. *Appl. Phys. Lett.* **2012**, *100*, 121106.
(43) Dalacu, D.; Mnaymneh, K.; Wu, X.; Lapointe, J.; Aers, G. C.; Poole, P. J.; Williams, R. L. Selective-Area Vapor-Liquid-Solid Growth of Tunable InAsP Quantum Dots in Nanowires. *Appl. Phys. Lett.* **2011**, *98*, 251101.
(44) Warburton, R. J. Single Spins in Self-Assembled Quantum Dots. *Nat. Mater.* **2013**, *12*, 483−493.
(45) Robinson, H. D.; Goldberg, B. B. Light-Induced Spectral Diffusion in Single Self-Assembled Quantum Dots. *Phys. Rev. B: Condens. Matter Mater. Phys.* **2000**, *61*, R5086−R5089.
(46) Reece, P. J.; Paiman, S.; Abdul-Nabi, O.; Gao, Q.; Gal, M.; Tan, H. H.; Jagadish, C. Combined Optical Trapping and Microphotoluminescence of Single InP Nanowires. *Appl. Phys. Lett.* **2009**, *95*, 101109.
(47) Wallentin, J.; Ek, M.; Wallenberg, L. R.; Samuelson, L.; Borgström, M. T. Electron Trapping in InP Nanowire Fets with Stacking Faults. *Nano Lett.* **2012**, *12*, 151−155.
(48) Haffouz, S.; Zeuner, K. D.; Dalacu, D.; Poole, P. J.; Lapointe, J.; Poitras, D.; Mnaymneh, K.; Wu, X.; Couillard, M.; Korkusinski, M.; Schöll, E.; Jöns, K. D.; Zwiller, V.; Williams, R. L. Bright Single InAsP Quantum Dots at Telecom Wavelengths in Position-Controlled InP Nanowires: The Role of the Photonic Waveguide,. *Nano Lett.* **2018**, *18*, 3047−3052.
(49) Foster, A. P.; Bradley, J. P.; Gardner, K.; Krysa, A. B.; Royall, B.; Skolnick, M. S.; Wilson, L. R. Linearly Polarized Emission from an Embedded Quantum Dot Using Nanowire Morphology Control. *Nano Lett.* **2015**, *15*, 1559−1563.
(50) van Weert, M. H. M.; Akopian, N.; Kelkensberg, F.; Perinetti, U.; van Kouwen, M. P.; Borgström, M. T.; Algra, R. E.; Verheijen, M. A.; Bakkers, E. P. A. M.; Kouwenhoven, L. P.; Zwiller, V. Orientation-Dependent Optical-Polarization Properties of Single Quantum Dots in Nanowires. *Small* **2009**, *5*, 2134−2138.
(51) Yang, S.; Dou, X.-M.; Yu, Y.; Ni, H.-Q.; Niu, Z.-C.; Jiang, D.-S.; Sun, B.-Q. Single-Photon Emission from GaAs Quantum Dots Embedded in Nanowires. *Chin. Phys. Lett.* **2015**, *32*, 077804.

https://doi.org/10.1021/acsami.1c21013
ACS Appl. Mater. Interfaces 2022, 14, 12488−12494